CHEMISTRY OF MATERIALS

pubs.acs.org/cm

Article

Synthesis and Properties of Monolayer Graphene (MLG)-Covered Fe(111)

Jeongmin Hong,* Han-Na Hwang, Yurong Su, Shihao Li, Jinghua Liang, Youngsin Park, Laishram T. Singh, Yong Gyun Jung, Ji-Hoon Yang, Jae-In Jeong, Hongxin Yang, Jeffrey Bokor, Chan-Cuk Hwang,* and Long You*

Cite This: *Chem. Mater.* 2020, 32, 10463−10468

Read Online

ACCESS | Metrics & More | Article Recommendations | Supporting Information

ABSTRACT: Fe undergoes a corrosion process under aerobic conditions. Oxidized forms of Fe lose malleability, durability, and other critical physical properties. For spintronic applications, alloy forms or capping layers are used to modulate the properties of Fe. Observing the Fe(111) spin structure is critical for practical applications. We suggest a method of coating Fe to retain its original magnetic properties. Thanks to monolayer graphene (MLG) growth, the properties of the Fe spin structure do not change, even under ambient conditions. Through angle-resolved photoemission spectroscopy (ARPES) and low-energy electron diffraction (LEED) measurements, we also found that interfacial band structures are modulated due to the presence of MLG.

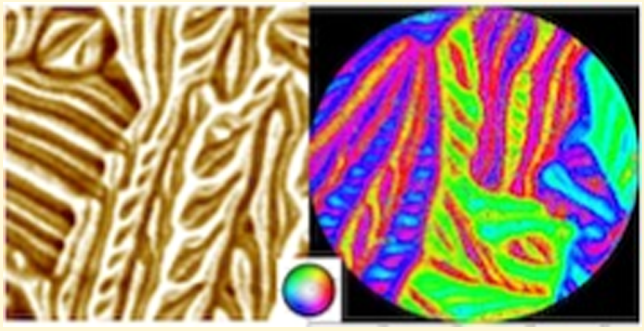

1. INTRODUCTION

Understanding the correlation between the magnetic domain structure and functional properties is important for materials subject to magnetic field-driven phase transitions or microstructure variations. Recently, many studies have been performed using two-dimensional (2D)-based materials with other metals for interfacial magnetic properties.[1−10] In this work, we report the synthesis of a monolayer of graphene (MLG) on single-crystalline Fe(111) by a chemical desorption process at 1000 K below the transition temperature. After MLG coating, the intrinsic magnetic and electronic properties of single-crystalline Fe(111) and the effects of MLG were investigated.

The magnetic easy axis lies on Fe(100), and the hard axis aligns on the (111) orientation. The magnetization of the Fe crystal along the (100) plane requires the least energy, whereas that along Fe(111) consumes the greatest amount of energy at approximately 3.5×10^{-6} eV per atom.[10] On the basis of the MLG-coated bcc-Fe(111) structure, it has been possible to engineer electronic and spin properties by manipulating the MLG and Fe(111) interface.

At the same time, the presence of MLG on Fe(111) prevents the oxidation of Fe and consequently preserves its unique properties, enabling the engineering of atomic spin structures. Once oxidized, the domain patterns realign in an energy-efficient manner, reducing domain walls as much as possible. Thus, the development of alternative forms of Fe−C-based materials is emerging in a timely manner. To this end, the adsorption of well-defined graphene under ultrahigh vacuum (UHV) conditions could be an excellent approach for engineering the electronic and magnetic properties of Fe. As previously reported, no impurities, even the smallest atoms, can penetrate graphene if close to a perfect crystalline monolayer of graphene is synthesized.[11]

Here, we report monolayer graphene growth on single-crystalline Fe(111). We observe the magnetic properties of single-crystalline Fe(111) and corrosive protection due to monolayer graphene. Monolayer graphene was grown by the dissociative adsorption of C_2H_2 under UHV conditions. Because graphene fully protects against oxidation, sharply branched three-dimensional (3D) magnetic domain patterns of Fe(111) were successfully observed. This combination of materials, with its aforementioned advantages, could be critical for many practical applications in future electronics.

2. RESULTS AND DISCUSSION

We synthesized a uniform structure of MLG on Fe(111) substrates. Compared with other synthesis methods, the dissociative adsorption of C_2H_2 is unique because it allows ultrahigh-quality graphene to be grown under UHV con-

Received: July 30, 2020
Revised: November 21, 2020
Published: December 3, 2020

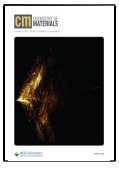

https://dx.doi.org/10.1021/acs.chemmater.0c03143
Chem. Mater. 2020, 32, 10463−10468

ditions.[15−18] The details of the synthesis are described in the Experimental Section.

The precleaning of Fe crystals before synthesis is a critical step. The upper image in Figure 1A shows the wide-scan

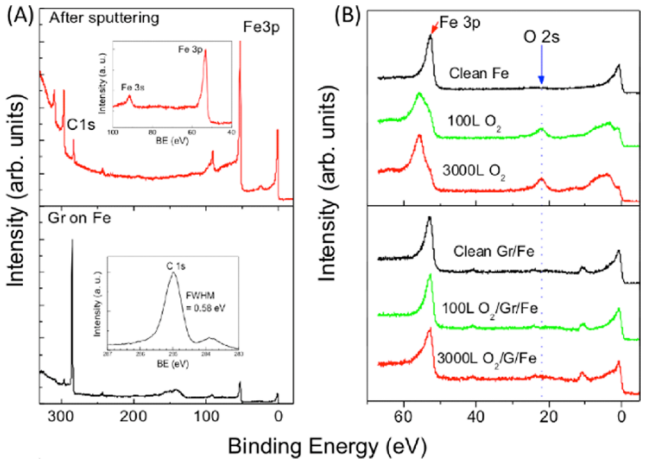

Figure 1. Synthesis of the MLG layer on top of the Fe surface. (A) PES spectra of pristine (upper) and MLG-coated (lower) Fe surfaces. The inset of the lower panel shows the **C** 1s peak in detail. (B) The PES results for pristine and MLG-coated Fe(111) surfaces after oxygen exposure up to 3000 L.

spectra of bare Fe(111). Repeated sputtering and annealing rendered the Fe substrate ultraclean, resulting in a spectrum with a relatively small **C** 1s peak and a strong **Fe** 3p peak near 50 eV. As shown in Figure 1A, after graphene formation (lower panel), the **C** 1s peak increased in intensity, while the **Fe** 3p peak weakened significantly. These results are a hallmark of MLG deposition and indicate that the Fe surface was covered with carbon atoms. A detailed view of this spectrum in a narrow range around the **C** 1s peak is shown in the inset of the lower panel. The full width at half-maximum (FWHM) of the **C** 1s peak is approximately 0.58 eV, indicating the formation of high-quality graphene. This peak is substantially narrower than that of CVD-grown graphene.[18]

Fe readily undergoes oxidation and corrosion, which strongly limits its use in many applications. Figure 1B shows the photoemission spectroscopy (PES) spectra of the clean and MLG-coated Fe surfaces with increasing O_2 exposure. The spectrum of the clean Fe surface (upper) shows a sharp **Fe** 3p peak at 52.5 eV, and no other peaks are observed. As shown in the lower panel of Figure 1B, however, when the surface is exposed to oxygen, the **O** 2s peak is observed at ∼21.95 eV, and the absorption of oxygen on the Fe surface substantially alters the valence band spectrum. The intensity of the **O** 2s peak is saturated when less than 100 L of oxygen is applied. The **Fe** 3p core-level peak also changes considerably due to the formation of bonds between the oxygen and Fe atoms.

By contrast, when the MLG-covered surface is exposed to oxygen, the **Fe** 3p peak remains nearly unchanged, and the **O** 2s peak is not visible even up to 3000 L. The results indicate that oxygen atoms cannot penetrate the graphene and that they do not combine with Fe atoms. We observed that MLG completely protects the Fe surface from oxidation. This protective effect was also confirmed by the ferroxyl test, as described in the Supporting Information Section (SI).

Scanning tunneling microscopy (STM) imaging under ambient conditions can identify pristine graphene structures.[19] Our analysis confirmed that the synthesized graphene is very smooth, as observed in the spectra shown in Figure 1. The inset image in Figure 2A shows branch-like lines that reflect the

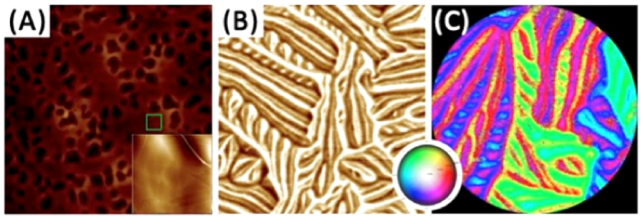

Figure 2. Surface measurements of MLG-covered Fe(111). (A) Atomic force microscopy (AFM) image and (B) the resultant magnetic force microscopy (MFM) images of the same structures under ambient conditions. The image dimensions are 5 × 5 μm^2. The inset shows an ambient STM image of monolayer graphene on single-crystalline Fe(111) (200 × 200 nm^2 image). (C) A micrograph of the domain structures acquired via spin-polarized low-energy electron microscopy (SPLEEM). The domain patterns show randomly oriented, sharply branched domain structures. The field of view (FOV) is 8 μm.

step-edge structure of Fe under the graphene layer. This result confirms the occurrence of the Fe(111) orientation and the thermal effects during the synthesis. The topographical image originates from the Fe−graphene interface.

The occurrence of interface dynamics during graphene growth can be inferred. Graphene forms two main domains oriented at approximately ±15° with respect to the substrate, and effects resulting from the adsorption energy difference and thermal annealing of the Fe crystal structure are observed. Kinetic roughening could drive random growth at the surfaces and interfaces in a certain way. The origin of this phenomenon is attributed to the domain rotation and kinetic roughening of graphene and Fe.[20,21]

Ultrahigh-sensitivity magnetic force microscopy (MFM) images collected under ambient conditions show unique domain structures (Figure 2B).[22−25] The magnetic domain patterns show multiple sharply branched tree-like structures. Since several domain walls are not thermodynamically favorable, the reduction of the walls stabilizes with a low-energy structure (more favorable). As reported in the literature, monolayer graphene does not exhibit ordered magnetic properties; instead, it prevents the oxidation of Fe substrates. Other types of Fe and Fe-based systems show similar patterns,[26,27] but graphene on Fe completely prevents other changes in domain patterns, such as oxidation.

To further investigate the magnetic orientation, we performed a spin-polarized low-energy electron microscopy (SPLEEM) experiment under UHV conditions. The results reveal unique domain patterns in a system without requiring the exposure of the sample to a magnetic field. SPLEEM produces clear images of the domain structures of Fe(111) with different magnetic orientations. The color scale in Figure 2C indicates the magnetic orientations from 0 to 360° in the image. These types of unique domain patterns were also observed in pristine Fe(111) after argon annealing and sputtering were performed under ambient and UHV conditions.

Figure 3A shows a schematic model of the Fe(111) structure. The Fe(111) substrate is modeled as six layers of an Fe crystal. The length of the basic vector in the primitive

https://dx.doi.org/10.1021/acs.chemmater.0c03143
Chem. Mater. 2020, 32, 10463−10468

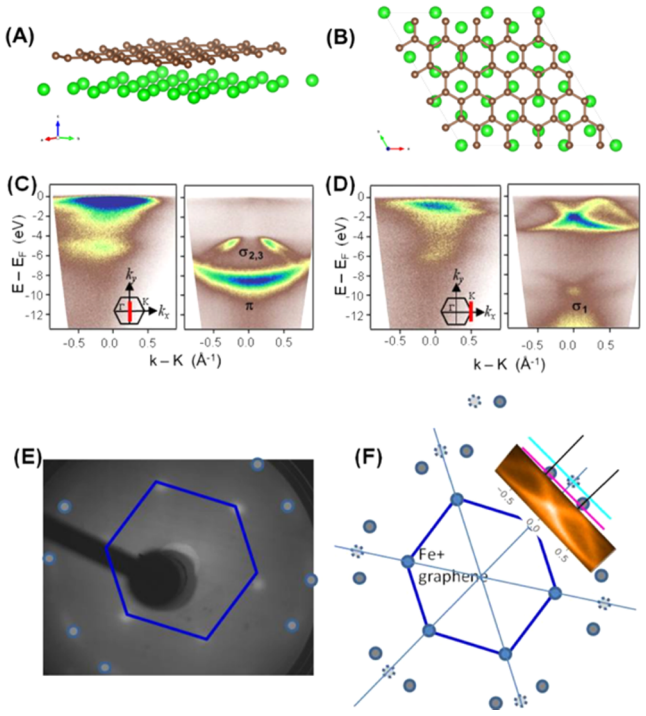

Figure 3. Schematic illustrations of the material structures and the formation of the layers and the resulting band structures: (A) Schematic of the MLG-Fe(111) structure. (B) Model of the MLG on Fe(111) structure. Angle-resolved photoemission spectroscopy (ARPES) images of (C) bare Fe(111) and (D) MLG-Fe(111) around the *K* point. (E) The low-energy electron diffraction (LEED) pattern of graphene on Fe(111). (F) The pattern shows two separately rotated domains. The ARPES results also show dual π bands, consistent with the LEED results.

surface unit cell of the Fe(111) film (a = 4.05 Å) is approximately 1.6 times larger than that of graphene (a = 2.46 Å). The graphene on the Fe(111) structure is illustrated in Figure 3B. We modeled different scenarios as described in the SI and found that the structure consumed the lowest energy. Accordingly, we studied the MLG-Fe(111) system, in which the lattice mismatch is reduced to less than 2%. Therefore, only interface effects were considered in the calculation.

Figure 3C presents the band structures of bare Fe(111) (left panel) and MLG-Fe(111) (right panel) around the Γ point of the Brillouin zone. The $\sigma_{2,3}$ and π bands of graphene are clearly observed, and the binding energies of these states are observed at ∼4.5 and ∼8.5 eV below the Fermi energy, respectively. The band structures of pristine Fe and MLG/Fe(111) around the *K* point are presented in Figure 3D (left and right panels, respectively). Figure 3D shows two clear π bands near the Fermi level, indicating that high-quality graphene was synthesized on the Fe(111) surface. The interaction energy between graphene and Fe(111) is stronger than that between graphene and other transition metals, such as Ni and Co.[16,17] Two different π bands arise from two separately rotated graphene domains. The rotation of the band dispersion is a signature of dual domains. In addition, two parabolic σ_1 bands are observed, analogous to the two π bands. The minima of the σ_1 bands around the *K* point are measured to lie at ∼10 eV below the Fermi energy. Multiple rotations of graphene have been similarly reported for graphene/Cu(111).[18]

Figure 3E shows the low-energy electron diffraction (LEED) pattern of MLG/Fe(111). The hexagonal lattice structure arises from bcc-Fe(111). The other spots, A and B, indicate the formation of two rotated graphene structures on Fe(111).[28,29] The rotation angle with respect to the hexagon of Fe(111) is approximately ±15°. To better understand the rotation angle, Figure 3F shows angle-resolved photoemission spectroscopy (ARPES) and LEED patterns together. The rotation angle is consistent with the ARPES results.

We swept a magnetic field with respect to the magnetization at the **Fe** $L_{3,2}$-edge, as shown in Figure 4A. The hysteresis

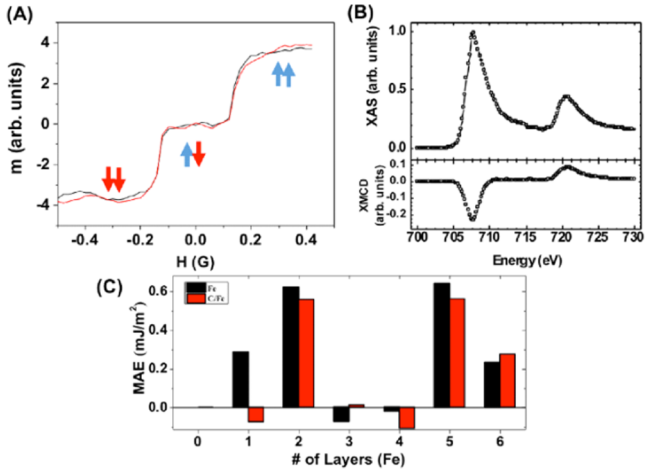

Figure 4. m−H loops of the structure and the calculated and experimental X-ray spectra. (A) m−H loops of the structure in the IP orientation. (B) XAS and XMCD spectra of Fe(111) after graphene growth. The penetration depth of the X-ray is less than 7 nm. (C) First-principles calculation of the interface-induced MAE of graphene on the Fe(111) structure.

loops indicate completely canted magnetization within the range of ±150 mT. The remanence within this range is zero. The plot is linear in the out-of-plane (OOP) component, indicating a hard axis. The interfaces are magnetically coupled to each other with zero remanence in this range, and for this reason, unique domain patterns are presented. By contrast, the OOP components only show a hard axis, very similar to the behavior of bulk Fe(111).

As shown in Figure 4B, the X-ray absorption spectroscopy (XAS) and X-ray magnetic circular dichroism (XMCD) spectra of the Fe $L_{3,2}$ edge present typical metallic behaviors without peak splitting or any signs of oxidation, although the system was exposed to air. The MLG membrane served as a coating to prevent any strong reaction or change in the interface anisotropy of Fe(111). For bcc-Fe, K_1 is positive, and Fe(100) is the favorable direction.

The highest density of atoms is in the (111) direction; consequently, the (111) axis is the hard axis, while (110) and (100) are the easy axes. The antiparallel magnetization directions are crystallographically equivalent, providing three distinct easy directions for positive-K_1 systems.

A first-principles calculation was performed, and the results showed that the MAE was reduced after the growth of the graphene interfaces. The topmost monolayer of Fe is coupled to graphene, changing the MAE in the other direction. Only the first layer will have some effects: the other layers show no significant effects. The calculation procedure is detailed in the Experimental Section. The canted magnetization from the m−H loops is correlated with randomly oriented tree-like domain patterns, as shown in Figure 2. Figure 4C shows the main

https://dx.doi.org/10.1021/acs.chemmater.0c03143
Chem. Mater. 2020, 32, 10463−10468

results, and the non-self-consistent total energy of the system was determined for the IP and OOP orientations of the magnetic moments. Couplings between MLG and transition metals due to proximity effects have been reported in the literature.[30,31]

Furthermore, the step-edge energy underneath the graphene layer induces atomic modulation and enhances the corrugation of the Fe surface during the annealing process. The surface morphology changes slightly due to lattice mismatch. Due to the MLG coating, we observe that the Fe system changes to show unique domain patterns. This modification allows closed 90° domains and unique domain structures in the Fe(111) orientation.

3. CONCLUSIONS

MLG on single-crystalline Fe(111) was successfully studied. High-quality MLG growth is possible through dissociative adsorption under UHV conditions. Because of the presence of graphene, a single-crystalline Fe(111) substrate can retain its original properties because it is prevented from reacting with the oxygen in the air. Due to the unique properties of the Fe structures, large numbers of randomly oriented domain walls are observed. In a magnetic field range of ±150 mT, the IP orientation is completely canted (coupled with the first layer of Fe atoms). If the thin-film types of the structures are patterned along the domains, then high-quality devices can be simply fabricated by growing MLG on top of the surface.[28]

4. EXPERIMENTAL SECTION

4.1. Fabrication of Monolayer Graphene onto Single-Crystalline Fe(111). A clean Fe(111) surface was prepared by applying multiple successive cycles of Ar^+ sputtering at an energy of 1 keV for 30 min over ∼24 h and subsequent annealing for 2−5 min at approximately 1000 K in a UHV chamber; this procedure was performed until carbon was minimized and no peaks corresponding to contaminants such as S, NO_2, or O_2 were observed by PES. After additional confirmation of the surface purity with LEED and ARPES, a graphene layer was grown on the Fe(111) substrate at ∼1000 K in a C_2H_2 atmosphere of 1×10^{-6} to 5×10^{-6} Torr.

4.2. ARPES and X-ray Photoelectron Spectroscopy (XPS) Measurements. The ARPES studies were performed at beamline 10D of the Pohang Accelerator Laboratory (PAL), which is equipped with a Scienta R4000 analyzer that provides an overall energy resolution of ∼50 meV at ∼34 eV under a pressure of 1.2×10^{-10} Torr. The binding energy was calibrated by measuring the Au Fermi energy and the Au 4f core-level spectrum. The data were collected at room temperature. The electronic band structures were taken from the clean Fe(111) surface and from the graphene grown on Fe(111) at the Γ and *K* points along the k_y direction in momentum space, as shown in the insets of Figure 1C,D. A photon energy of 420 eV was used for spectrum collection.

4.3. Ferroxyl Spray Test. The ferroxyl test was conducted while monitoring the appearance of the Fe surface. The test solution was sprayed onto the surfaces of the bare Fe and the graphene-coated structure.

4.4. Scanning Probe Microscopy (SPM) and Scanning Tunneling Microscopy (STM). SPM and magnetic force microscopy (MFM) were performed via 30 nm dynamic mode scanning. STM was used for high-quality topographic measurements under ambient conditions.

4.5. Spin-Polarized Low-Energy Electron Microscopy (SPLEEM). Real-space images were acquired using three orthogonal electron beam spin alignments such that the magnetic contrast along three orthogonal directions corresponds to the OOP magnetization direction and two orthogonal IP axes. SPLEEM images map the magnetization of the sample in the sense that the intensity in each pixel represents the dot product of the spin polarization vector **P** of the illumination beam and the magnetization vector **M** with a lateral resolution on the order of 10 nm.

4.6. First-Principles Calculation. In the framework of density functional theory, our first-principles calculation was performed using the Vienna ab initio simulation package (VASP) with the Perdew−Burke−Ernzerhof generalized gradient approximation (GGA-PBE).[12,13] The electron−ion interaction is described by the projected augmented wave (PAW) potentials.[14] In all calculations, a kinetic energy cutoff of 520 eV and a Γ-centered 6 × 6 × 1 *K*-point mesh for the first Brillouin zone integration are employed. The MAE is calculated in three steps. First, structural relaxation is performed until the forces on each atom are smaller than 0.001 eV/Å to determine the ground state. Next, the Kohn−Sham equations are solved with no spin−orbit coupling (SOC) considered to determine the charge distribution of the system's ground state. Finally, the SOC is included, and the non-self-consistent total energy of the system is determined when the orientations of the magnetic moments are set for both IP and OOP.

Understanding the correlation between the magnetic domain structure and functional properties is important for materials subject to magnetic field-driven phase transitions or microstructure variations. Recently, many studies have been performed using 2D-based materials with other metals for interfacial magnetic properties. In this work, we report the synthesis of a monolayer of graphene (MLG) on single-crystalline Fe(111) by a chemical desorption process at 1000 K below the transition temperature. After MLG coating, the intrinsic magnetic and electronic properties of single-crystalline Fe(111) and the effects of MLG were investigated.

■ ASSOCIATED CONTENT

Supporting Information

The Supporting Information is available free of charge at https://pubs.acs.org/doi/10.1021/acs.chemmater.0c03143.

Additional characterization and calculation results (Figures S1−S3) (PDF)

■ AUTHOR INFORMATION

Corresponding Authors

Jeongmin Hong − *School of Optical and Electronic Information, Huazhong University of Science and Technology, Wuhan 430074, China; EECS, UC Berkeley, Berkeley, California 94720, United States;* orcid.org/0000-0002-8639-3620; Email: jehong@hust.edu.cn

Chan-Cuk Hwang − *Pohang Accelerator Laboratory (PAL), Pohang University of Science and Technology, Pohang 37673, South Korea*; Email: cchwang@postech.ac.kr

Long You − *School of Optical and Electronic Information, Huazhong University of Science and Technology, Wuhan 430074, China;* orcid.org/0000-0001-5713-194X; Email: lyou@hust.edu.cn

Authors

Han-Na Hwang − *Pohang Accelerator Laboratory (PAL), Pohang University of Science and Technology, Pohang 37673, South Korea*

Yurong Su − *School of Optical and Electronic Information, Huazhong University of Science and Technology, Wuhan 430074, China;* orcid.org/0000-0003-2237-9771

Shihao Li − *School of Optical and Electronic Information, Huazhong University of Science and Technology, Wuhan 430074, China*

Jinghua Liang − *Key Laboratory of Magnetic Materials and Devices, Ningbo Institute of Materials Technology and Engineering, Chinese Academy of Sciences, Ningbo 315201, China*

https://dx.doi.org/10.1021/acs.chemmater.0c03143
Chem. Mater. 2020, 32, 10463−10468

Youngsin Park − *School of Natural Science, UNIST, Ulsan 44919, South Korea;* orcid.org/0000-0002-1789-750X
Laishram T. Singh − *Pohang Accelerator Laboratory (PAL), Pohang University of Science and Technology, Pohang 37673, South Korea*
Yong Gyun Jung − *Steel Solution Marketing Planning Group, POSCO, Seoul 06194, South Korea*
Ji-Hoon Yang − *Research Institute of Industrial Science and Technology (RIST), Pohang 37673, South Korea*
Jae-In Jeong − *Research Institute of Industrial Science and Technology (RIST), Pohang 37673, South Korea*
Hongxin Yang − *Key Laboratory of Magnetic Materials and Devices, Ningbo Institute of Materials Technology and Engineering, Chinese Academy of Sciences, Ningbo 315201, China*
Jeffrey Bokor − *EECS, UC Berkeley, Berkeley, California 94720, United States*

Complete contact information is available at: https://pubs.acs.org/10.1021/acs.chemmater.0c03143

Author Contributions

J.H. and C.-C.H. conceived the idea and initiated the research. The manuscript was written through contributions of all authors.

Notes

The authors declare no competing financial interest.

■ ACKNOWLEDGMENTS

This work was supported by the National Natural Science Foundation of China under Award number 61674062 and the U.S. Department of Energy, Office of Basic Energy Sciences Division of Materials Sciences and Engineering under Contract No. DE-AC02-05CH11231. The authors also acknowledge financial support from the National Science Foundation (NSF) under Award number 0939514 and the National Research Foundation of Korea supported by the Korean Government (Ministry of Science and ICT) #2018R1A5A6075964, #2020R1A2B5B02001876, #2017M3A7B4049173, and #2020M3D1A1110548.

■ REFERENCES

(1) McGuire, M. A.; Dixit, H.; Cooper, V. R.; Sales, B. C. Coupling of crystal structure and magnetism in the layered, ferromagnetic insulator CrI3. *Chem. Mater.* **2015**, *27*, 612−620.
(2) Liu, J. Y.; Sun, Q.; Kawazoe, Y.; Jena, P. Exfoliating biocompatible ferromagnetic Cr-trihalide monolayers. *Phys. Chem. Chem. Phys.* **2016**, *18*, 8777−8784.
(3) Huang, B.; et al. Layer-dependent ferromagnetism in a van der Waals crystal down to the monolayer limit. *Nature* **2017**, *546*, 270−273.
(4) Gong, C.; Li, L.; Li, Z.; Ji, H.; Stern, A.; Xia, Y.; et al. Discovery of intrinsic ferromagnetism in two-dimensional van der Waals crystals. *Nature* **2017**, *546*, 265−269.
(5) Klein, D. R.; et al. Probing magnetism in 2D van der Waals crystalline insulators via electron tunneling. *Science* **2018**, *360*, No. eaar3617.
(6) van't Erve, O. M. J.; Friedman, A. L.; Cobas, E.; Li, C. H.; Robinson, J. T.; Jonker, B. T. Low-resistance spin injection into silicon using graphene tunnel barriers. *Nat. Nanotechnol.* **2012**, *7*, 737−742.
(7) Sepioni, M.; Nair, R. R.; Rablen, S.; Narayanan, J.; Tuna, F.; Winpenny, R.; et al. Limits on intrinsic magnetism in graphene. *Phys. Rev. Lett.* **2010**, *105*, No. 207205.
(8) Nair, R. R.; Sepioni, M.; Tsai, I. L.; Lehtinen, O.; Keinonen, J.; Krasheninnikov, A. V.; et al. Spin-half paramagnetism in graphene induced by point defects. *Nat. Phys.* **2012**, *8*, 199−202.
(9) Ghazaryan, D.; Greenaway, M. T.; Wang, Z.; Guarochico-Moreira, V. H.; Vera-Marun, I. J.; Yin, J.; et al. Magnon-assisted tunneling in van der Waals heterostructures based on CrBr3. *Nat. Electron.* **2018**, *1*, 344−349.
(10) Vonsovskii, S. V. *Magnetism*; Nauka: Moscow, 1971.
(11) Bunch, J. S.; Verbridge, S. S.; Alden, J. S.; van der Zande, A. R.; Parpla, J. M.; Craighead, H. G.; et al. Impermeable atomic membranes from graphene sheets. *Nano Lett.* **2008**, *8*, 2458−2462.
(12) Kresse, G.; Furthmüller, J. Efficient iterative schemes for ab initio total-energy calculations using a plane-wave basis set. *Phys. Rev. B* **1996**, *54*, No. 11169.
(13) Perdew, J. P.; Burke, K.; Ernzerhof, M. Generalized Gradient Approximation Made Simple. *Phys. Rev. Lett.* **1996**, *77*, No. 3865.
(14) Blöchl, P. E. Projector augmented-wave method. *Phys. Rev. B* **1994**, *50*, No. 17953.
(15) Kayastha, V.; Yap, Y. K.; Dimovski, S.; Gogotsi, Y. Controlling dissociative adsorption for effective growth of carbon nanotubes. *Appl. Phys. Lett.* **2004**, *85*, No. 3265.
(16) Mittendorfer, F.; Garhofer, A.; Redinger, J.; Klimes, J.; Harl, J.; Kresse, G. Graphene on Ni(111): Strong interaction and weak adsorption. *Phys. Rev. B* **2011**, *84*, No. 201401.
(17) Li, X.; Cai, W.; An, J.; Kim, S.; Nah, J.; Yang, D.; et al. Large-area synthesis of high-quality and uniform graphene films on copper foils. *Science* **2009**, *324*, 1312−1314.
(18) Jeon, C.; Hwang, H. N.; Lee, W. G.; Jung, Y. G.; Kim, K. S.; Park, C. Y.; et al. Rotated domains in chemical vapor deposition-grown monolayer graphene on Cu(111): an angle-resolved photoemission study. *Nanoscale* **2013**, *5*, 8210−8214.
(19) Hong, J.; Bekyarova, E.; Liang, P.; deHeer, W. A.; Haddon, R. C.; Khizroev, S. Room-temperature magnetic ordering in functionalized graphene. *Sci. Rep.* **2012**, *2*, No. 624.
(20) Laurila, T.; Tong, C.; Huopaniemi, I.; Majaniemi, S.; Ala-Nissila, T. Dynamics and kinetic roughening of interfaces in two-dimensional forced wetting. *Eur. Phys. J. B* **2005**, *46*, 553−561.
(21) Krim, J.; Palasantzas, G. Experimental observations of self-affine scaling and kinetic roughening at sub-micron lengthscales. *Int. J. Mod. Phys. B* **1995**, *09*, 599.
(22) Hong, J.; Niyogi, S.; Bekyarova, E.; Itkis, M. E.; Ramesh, P.; Amos, N.; et al. Effect of nitrophenyl functionlization on the magnetic properties of epitaxial graphene. *Small* **2011**, *7*, 1175−1180.
(23) Niyogi, S.; Bekyarova, E.; Hong, J.; Khizroev, S.; Berger, C.; de Heer, W. A.; et al. Covalent chemistry for graphene electronics. *J. Phys. Chem. Lett.* **2011**, *2*, 2487−2498.
(24) Hong, J.; Bekyarova, E.; de Heer, W. A.; Haddon, R. C.; Khizroev, S. Chemically engineered graphene-based 2D organic molecular magnet. *ACS Nano* **2013**, *7*, 10011−10022.
(25) Hong, J.; Kim, Y.; Liang, J.; Chen, H.; Park, C. Y.; Yang, H.; et al. Intrinsic controllable magnetism of graphene grown on Fe. *J. Phys. Chem. C* **2019**, *123*, 26870−26876.
(26) Santos, B.; Loginova, E.; Mascaraque, A.; de la Figuera, J.; et al. Structure and magnetism in ultrathin iron oxides characterized by low energy electron microscopy. *J. Phys.: Condens. Matter* **2009**, *21*, No. 314011.
(27) Ruiz-Gómez, S.; Perez, L.; Mascaraque, A.; Quesada, A.; Prieto, P.; Palacio, I.; et al. Geometrically defined spin structures in ultrathin Fe3O4 with bulk like magnetic properties. *Nanoscale* **2018**, *10*, 5566−5573.
(28) Pletikosić, I.; Kralj, M.; Pervan, P.; Brako, R.; Coraux, J.; N'Diaye, A. T.; et al. Dirac cones and minigaps for graphene on Ir(111). *Phys. Rev. Lett.* **2009**, *102*, No. 056808.
(29) Coraux, J.; N'Diaye, A. T.; Busse, C.; Michely, T. Structural coherency of graphene on Ir(111). *Nano Lett.* **2008**, *8*, 565−570.
(30) Leutenantsmeyer, J. C.; Kaverzin, A. A.; Wojtaszek, M.; van Wees, B. J. Proximity induced room temperature ferromagnetism in graphene probed with spin currents. *2D Mater.* **2017**, *4*, No. 014001.

(31) Wang, Z.; Tang, C.; Sachs, R.; Barlas, Y.; Shi, J. Proximity-induced ferromagnetism in graphene revealed by the anomalous Hall effect. *Phys. Rev. Lett.* **2015**, *114*, No. 016603.

https://dx.doi.org/10.1021/acs.chemmater.0c03143
Chem. Mater. 2020, 32, 10463−10468